

Complete Source Trajectories for C-Arm Systems and a Method for Coping with Truncated Cone-Beam Projections

Hermann Schomberg

Philips Research Hamburg, Röntgenstraße 24–26, 22335 Hamburg, Germany

1 Introduction

A C-arm system, such as the one shown in Figure 1, may be used to acquire X-ray cone-beam projections of a patient's three-dimensional (3D) region of interest (ROI) while the X-ray source moves along some trajectory around the ROI. Then, a 3D image of the X-ray attenuation coefficient within the ROI may be reconstructed from the acquired cone-beam projections.

In fact, C-arm systems are being used in this way, see e.g. [1, 2]. Typically, the source moves along a circular arc spanning an angle of 180° – 200° , and the image is reconstructed by a variant of the algorithm of Feldkamp, Davis, and Kress [3]. As the cone-beam does not cover the whole patient, the projections are truncated. This is usually handled by extending the projections in a simple manner parallel to the plane containing the source trajectory. In practice, the true trajectory differs slightly from its ideal, but this deviation can be measured [5, 6] and taken into account during the reconstruction. The reconstructed image is subjected to a surface or volume rendering process designed to extract and visualize only the high contrast structures of the object under examination.

The reconstructed image itself is usually cluttered by severe artifacts. Nevertheless, the high contrast structures, such as bones or blood vessels filled with intraarterially injected contrast agents, are well recovered. This is because such structures stand out well against the background and are also reconstructed at the correct geometric locations.

Accurate images of medium contrast structures, such as blood vessels filled with intravenously injected contrast agents, or low contrast structures, such as soft tissue organs, are not obtained in this way. If this is to be improved upon, the following conditions will have to be met: First, the data acquired by the C-arm system must provide (after some preprocessing) accurate, though sampled, cone-beam projections of the object function (the X-ray attenuation coefficient). Second, the sampling density along the trajectory and on the detector surface must be sufficiently high. Third, the source trajectory must be complete in the sense that every plane that intersects the ROI contains a source point. Fourth, the cone beam projections must not be truncated. Under these conditions, any standard exact cone-beam reconstruction algorithm will produce an accurate estimate of the object function within the ROI. It has been tacitly assumed that the object function varies only spatially. Imaging moving parts of the human body, such as the beating heart, is not considered here.

Measuring accurate cone-beam projections of the object function presents a number of technical challenges, but no fundamental obstacles, and is also not considered here. Making the sampling density sufficiently high is not a fundamental problem either. The problem of designing source trajectories that are both complete and realizable by appropriate C-arm systems is discussed and solved in Section 4. The remaining requirement for non-truncated cone beam projections cannot be satisfied by any realistic C-arm system when the object to be imaged is part of

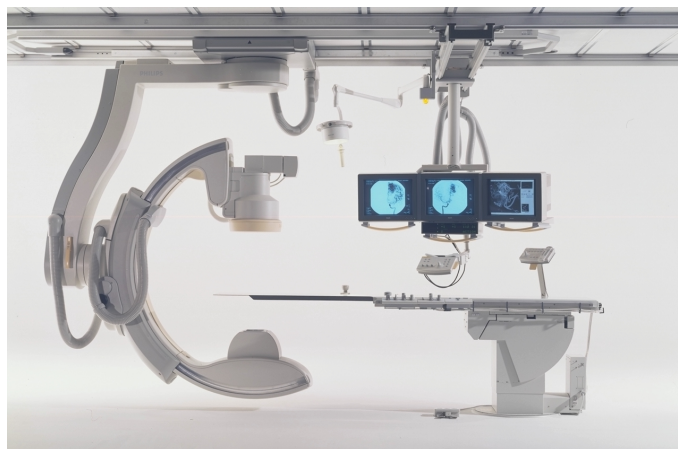


Figure 1. Integris Allura C-arm system (Philips Medical Systems, Best, The Netherlands).

a human body. As in the fan-beam case [4] one can show that truncated cone-beam projections leave the object undetermined. To cope with this fundamental limitation we suggest in Section 3 to extend the truncated projections in a relatively simple fashion so as to fake non-truncated projections of an imaginary object that is somewhat bigger than the ROI, and to apply a suitable cone-beam reconstruction algorithm to the extended projections. It will be argued in Section 3 that an image thus obtained can be expected to differ, inside the ROI, from the true image merely by some unknown, but smooth, nearly constant, and fairly weak ghost image. The reconstructed image would therefore still allow the detection of fine anatomical details.

2 C-Arm Systems

A typical C-arm system, such as the one shown in Figure 1, is equipped with a point like X-ray source and a planar X-ray detector, usually an image intensifier, which are mounted to the ends of a C-arm. The C-arm is held by another arm, which we refer to as the C-arm suspension. The C-arm suspension is attached to an L-arm, which is mounted to the ceiling (or floor). The L-arm can be rotated about a vertical axis. The C-arm suspension can be rotated about a horizontal axis attached to the L-arm. By rotating L-arm and C-arm suspension about their axes, the orientation of the plane containing the C-arm may be changed. The C-arm itself may be rotated within this plane about an axis perpendicular to this plane. All three rotation axes meet in a single point, the isocenter. Also, the straight line from the X-ray source to the center of the detector surface passes through the isocenter. The rotations themselves are effected by servo motors. When one or more of the the arms rotate, the X-ray source moves along a corresponding trajectory. The trajectory is confined to the surface of an isocentric sphere and further constrained by the electromechanical design of the joints connecting the arms.

3 The Reconstruction Problem

Points in space will be referenced with respect to a right-handed Cartesian coordinate system, the laboratory system, which we attach to the isocenter of the C-arm system such that the z -axis points upwards and the y -axis along the patient table. The object to be imaged is represented by a function $f : \mathbf{R}^3 \rightarrow \mathbf{R}$. The source trajectory is represented by a smooth mapping $\mathbf{a} : \Lambda \rightarrow \mathbf{R}^3$, where $\Lambda = [\lambda_-, \lambda_+]$ is a bounded interval. When the source is at position $\mathbf{a}(\lambda)$, the sensitive area of the detector defines a plane $D(\lambda) \subset \mathbf{R}^3$. The sensitive area of the detector itself is represented by the disk $D_0(\lambda) \subset D(\lambda)$. The set of unit vectors $\boldsymbol{\theta} \in S^2$ such that the ray $\{\mathbf{a}(\lambda) + s\boldsymbol{\theta} \mid s \geq 0\}$ hits $D_0(\lambda)$ is denoted by $S_0(\lambda)$. The source point $\mathbf{a}(\lambda)$ and the unit vectors in $S_0(\lambda)$ define the cone $C_0(\lambda) = \{\mathbf{a}(\lambda) + s\boldsymbol{\theta} \mid s \geq 0, \boldsymbol{\theta} \in S_0(\lambda)\}$. The biggest centered ball contained in all cones $C_0(\lambda)$, $\lambda \in \Lambda$, is denoted by B_0 , its radius by r_0 . This ball is also the biggest centered ball within which we can hope to obtain an accurate reconstruction. In practice, r_0 lies between 100 and 150 mm. We define the function $g : \Lambda \times S^2 \rightarrow \mathbf{R}$ by

$$g(\lambda, \boldsymbol{\theta}) = \int_0^\infty f(\mathbf{a}(\lambda) + s\boldsymbol{\theta}) ds. \quad (1)$$

The function $g(\lambda, \cdot)$ represents the (non-truncated) cone-beam projection of f with vertex $\mathbf{a}(\lambda)$. The data acquisition process provides (a sampled and noise contaminated version of) the function $\tilde{g}(\lambda, u, v) = g(\lambda, \tilde{\boldsymbol{\theta}}(\lambda, u, v))$, where (u, v) are local coordinates in the detector plane $D(\lambda)$ and $\tilde{\boldsymbol{\theta}}(\lambda, u, v) \in S_0(\lambda)$ is the unit vector pointing from $\mathbf{a}(\lambda)$ to the point (u, v) on $D_0(\lambda)$. Thus, $g(\lambda, \boldsymbol{\theta})$ is available only for $\lambda \in \Lambda$, $\boldsymbol{\theta} \in S_0(\lambda)$. Using these data, we wish to reconstruct f in the ball B_0 . When the object is a part of a human being, the acquired cone-beam projections are inevitably truncated, i.e., the support of f extends beyond B_0 , and there exist $\lambda \in \Lambda$ and $\boldsymbol{\theta} \in S^2 \setminus S_0(\lambda)$ such that $g(\lambda, \boldsymbol{\theta}) \neq 0$.

For a stable and accurate reconstruction of f in B_0 it is necessary that the source trajectory \mathbf{a} satisfy the following completeness condition (see [7] and the references cited therein): *Every plane that intersects the ball B_0 contains a source point $\mathbf{a}(\lambda)$.* A source trajectory satisfying this condition will be called complete with respect to B_0 . The normals of the planes that contain a source point $\mathbf{a}(\lambda)$ and intersect the ball B_0 form an umbrella-shaped surface

$$U(\lambda, r_0) = \{r\boldsymbol{\theta} \mid |r| \leq r_0, \boldsymbol{\theta} \in S^2, \mathbf{a}(\lambda) \cdot \boldsymbol{\theta} = r\} \quad (2)$$

within B_0 . Using the correspondence between planes and their normals, the completeness condition may be rephrased as follows: *The collection of the surfaces $U(\lambda, r_0)$, $\lambda \in \Lambda$, fills the ball B_0 completely.*

In general, it is hard to prove by argument that a given trajectory is complete with respect to B_0 . However, a computer may be used to draw a large number of surfaces $U(\lambda_0, r_0), \dots, U(\lambda_N, r_0)$ with $\lambda_n = n(\lambda_+ - \lambda_-)/N$, $n = 0, 1, \dots, N$, and it may be checked visually whether these surfaces will densely fill B_0 as $N \rightarrow \infty$.

In the remainder of this section, we assume that the source trajectory is complete with respect to B_0 . Then, if the cone-beam projections were not truncated, f could be reconstructed inside B_0 using an appropriate cone-beam reconstruction algorithm, such as the filtered backprojection algorithm described

in [8]. This algorithm is designed to act on $\tilde{g}(\lambda, u, v)$ rather than on $g(\lambda, \boldsymbol{\theta})$.

The development presented in [8] also allows one to derive the explicit reconstruction formula

$$f_{\text{rec}}(\mathbf{x}) = \frac{1}{8\pi^2} \int_\Lambda \int_{S^2} K(\mathbf{x}, \lambda, \boldsymbol{\theta}) g(\lambda, \boldsymbol{\theta}) d\boldsymbol{\theta} d\lambda \quad (3)$$

with the kernel

$$K(\mathbf{x}, \lambda, \boldsymbol{\theta}) = \int_{S^2} \frac{|\mathbf{a}'(\lambda) \cdot \boldsymbol{\beta}|}{\|\mathbf{x} - \mathbf{a}(\lambda)\|^2} M(\lambda, \boldsymbol{\beta}) \delta'_\epsilon(\boldsymbol{\beta} \cdot \boldsymbol{\phi}(\lambda, \mathbf{x})) \delta'_\epsilon(\boldsymbol{\beta} \cdot \boldsymbol{\theta}) d\boldsymbol{\beta}. \quad (4)$$

Here, \mathbf{a}' is the derivative of \mathbf{a} ; δ'_ϵ is a regular and smooth approximation to the derivative of the δ -function; M is a smooth weighting function accounting for the fact that a plane can contain several source points [7, 8]; and

$$\boldsymbol{\phi}(\lambda, \mathbf{x}) = \frac{\mathbf{x} - \mathbf{a}(\lambda)}{\|\mathbf{x} - \mathbf{a}(\lambda)\|}. \quad (5)$$

When the conditions are right, one expects f_{rec} to tend to f inside B_0 as δ'_ϵ tends to δ' . A discretized version of (3) could provide the basis for a (computationally inefficient) reconstruction algorithm.

More interestingly, the kernel (4) highlights an important property of the reconstruction problem: Since δ'_ϵ is concentrated near zero, $\delta'_\epsilon(\boldsymbol{\beta} \cdot \boldsymbol{\phi}(\lambda, \mathbf{x}))$ is appreciably nonzero only when $\boldsymbol{\beta}$ belongs to a neighborhood of the circle $S^2 \cap \boldsymbol{\phi}(\lambda, \mathbf{x})^\perp$, and $\delta'_\epsilon(\boldsymbol{\beta} \cdot \boldsymbol{\theta})$ is appreciably nonzero only when $\boldsymbol{\beta}$ belongs to a neighborhood of the circle $S^2 \cap \boldsymbol{\theta}^\perp$. The mentioned two circles are identical if $\boldsymbol{\theta}$ and $\boldsymbol{\phi}(\lambda, \mathbf{x})$ are parallel; otherwise they have only two points in common. As a result, $K(\mathbf{x}, \lambda, \boldsymbol{\theta})$ is appreciably nonzero at most when $\boldsymbol{\theta}$ and $\boldsymbol{\phi}(\lambda, \mathbf{x})$ are nearly parallel, i.e., when the ray $\{\mathbf{a}(\lambda) + s\boldsymbol{\theta} \mid s \geq 0\}$ comes close to \mathbf{x} . In addition, $K(\mathbf{x}, \lambda, \boldsymbol{\theta})$ depends smoothly and weakly on λ and $\boldsymbol{\theta}$ whenever \mathbf{a} depends smoothly on λ and the ray $\{\mathbf{a}(\lambda) + s\boldsymbol{\theta} \mid s \geq 0\}$ does not come close to \mathbf{x} . Although the reconstruction process is not strictly local, it is still semi-local.

The reconstruction problem of 2D CT has similar properties [9]. It is also possible to extend the ideas presented in [9] to the 3D case: From (3) we find that

$$f_{\text{rec}}(\mathbf{x}) = f_0(\mathbf{x}) + f_1(\mathbf{x}) \quad (6)$$

with

$$f_0(\mathbf{x}) = \frac{1}{8\pi^2} \int_\Lambda \int_{S_0(\lambda)} K(\mathbf{x}, \lambda, \boldsymbol{\theta}) g(\lambda, \boldsymbol{\theta}) d\boldsymbol{\theta} d\lambda, \quad (7)$$

$$f_1(\mathbf{x}) = \frac{1}{8\pi^2} \int_\Lambda \int_{S^2 \setminus S_0(\lambda)} K(\mathbf{x}, \lambda, \boldsymbol{\theta}) g(\lambda, \boldsymbol{\theta}) d\boldsymbol{\theta} d\lambda. \quad (8)$$

The function f_0 is well determined by the available data, but f_1 is completely undetermined. Owing to the semi-local nature of the reconstruction process, f_0 will be fairly smooth well outside B_0 and decay quickly there. Conversely, f_1 will be fairly smooth well within B_0 . Also, a crude guess of the truncated portions of the cone-beam projections should suffice to compute a fair approximation to f_1 inside B_0 . Already a crude guess of the

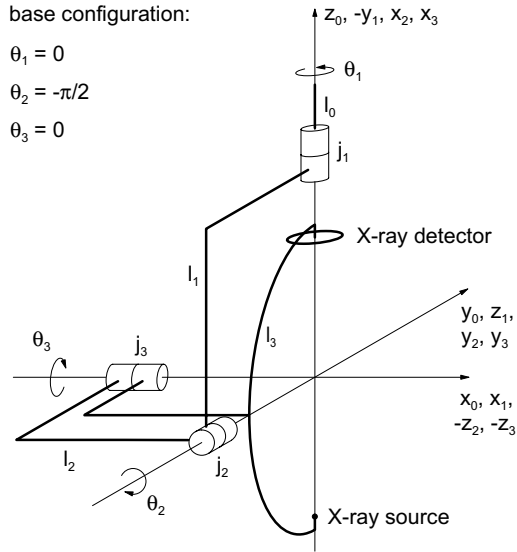


Figure 2. A C-arm system drawn as a series of links and joints.

integrals along the lines that pass through a centered ball B_1 a little larger than B_0 should suffice for this purpose.

These observations suggest the following method for coping with truncated cone-beam projections: 1. Choose a centered ball B_1 somewhat bigger than B_0 . For each $\lambda \in \Lambda$, let $D_1(\lambda)$ be the perspective projection of B_1 from $\mathbf{a}(\lambda)$ onto $D(\lambda)$. 2. Extend each truncated cone-beam projection $\tilde{g}(\lambda, \cdot, \cdot)$ radially from $D_0(\lambda)$ to $D_1(\lambda)$ using, for example, the 1D extension method proposed in [9] in radial direction. 3. Reconstruct f in B_0 by applying the filtered backprojection algorithm described in [8], or some other suitable cone-beam reconstruction algorithm, to the extended projections.

An image reconstructed in this way can be expected to differ inside B_0 from the true image merely by some unknown, but smooth, nearly constant, and fairly weak ghost image.

4 Complete Source Trajectories

To specify and design source trajectories, we adopt a method commonly used in robotics [10]. The first step is to model the C-arm system by a series of rigid links connected by revolute joints. Figure 2 illustrates the idea. There are four links, denoted by l_0, l_1, l_2, l_3 , and three joints, denoted by j_1, j_2, j_3 . Link l_0 is fixed to the laboratory. Link l_1 represents the L-arm, link l_2 the C-arm suspension, and l_3 the C-arm. Joint j_k connects links l_{k-1} and l_k , $k = 1, 2, 3$. Each joint defines an axis of rotation, and these axes intersect in the isocenter.

Next, a right-handed Cartesian (x_k, y_k, z_k) -coordinate system is attached to link l_k , $k = 0, 1, 2, 3$. There is some freedom in the choice of the origins and orientations of these coordinate systems; we make the choices indicated in Figure 2. In the jargon of robotics, the coordinate system attached to link l_3 is called the tool frame. The coordinate system attached to link l_0 is called the base frame and coincides with the laboratory system introduced in Section 3. The angle between the x_{k-1} -axis and the x_k -axis, measured about the z_{k-1} axis, is denoted by θ_k , $k = 1, 2, 3$. Each triple $(\theta_1, \theta_2, \theta_3)$ defines a configuration of the C-arm system. Figure 2 illustrates the configuration associated

with $(\theta_1, \theta_2, \theta_3) = (0, -\pi/2, 0)$.

A point in space may be specified by its coordinates in either of the four coordinate systems. It is explained in [10] how to transform the coordinates of the point from the tool frame to its coordinates in the base frame: If the point is represented by \mathbf{x}_3 in the tool frame, then it is represented by

$$\mathbf{x}_0 = \mathbf{R}(\theta_1, \theta_2, \theta_3)\mathbf{x}_3 \quad (9)$$

in the base frame, where $\mathbf{R}(\theta_1, \theta_2, \theta_3)$ is a rotation matrix. This matrix can be derived from the information provided in Figure 2 and is given by (see also example 3.3.3 in [10])

$$\mathbf{R}(\theta_1, \theta_2, \theta_3) = \begin{pmatrix} c_1 c_2 c_3 - s_1 s_3 & -c_1 c_2 s_3 - s_1 c_3 & c_1 s_2 \\ s_1 c_2 c_3 + c_1 s_3 & -s_1 c_2 s_3 + c_1 c_3 & s_1 s_2 \\ -s_2 c_3 & s_2 s_3 & c_2 \end{pmatrix}$$

with $c_k = \cos \theta_k$ and $s_k = \sin \theta_k$, $k = 1, 2, 3$.

In the tool frame, the source is always at position $\mathbf{x}_{\text{src}} = (-r_{\text{src}}, 0, 0)^T$, where r_{src} is the distance between source and isocenter. When the angles $\theta_1, \theta_2, \theta_3$ are chosen as functions of the parameter $\lambda \in \Lambda$, then \mathbf{x}_{src} moves along the trajectory

$$\mathbf{a}(\lambda) = \mathbf{R}(\theta_1(\lambda), \theta_2(\lambda), \theta_3(\lambda))\mathbf{x}_{\text{src}}, \quad \lambda \in \Lambda \quad (10)$$

in the base frame. Thus a trajectory may be specified by three angular functions $\theta_k(\lambda)$, $k = 1, 2, 3$.

To design trajectories that are complete with respect to B_0 , we may simply guess appropriate angular functions. Whether a candidate trajectory is complete with respect to B_0 may be checked as described in Section 3. The mechanical and electromechanical constraints of the C-arm system will have to be obeyed. Angle θ_1 is preferably chosen constant, but for a complete trajectory the other two angles must vary. Accordingly, the C-arm system must allow a simultaneous rotation of the C-arm and the C-arm suspension while cone-beam projections are being taken.

To realize a trajectory, the parameter λ is replaced by a smooth, monotonically increasing function of time, say $\tau : [t_-, t_+] \rightarrow \Lambda$, and the resulting functions $\theta_k(\tau(t))$ are used to drive the corresponding servo motors of the C-arm system. For physical reasons the first and second derivatives of the entailing trajectory $\mathbf{a}(\tau(t))$ must vanish as $t \downarrow t_-$ and $t \uparrow t_+$. This may be achieved by a proper choice of the function τ . Alternatively, the original trajectory may be augmented at both ends with extra segments for acceleration and deceleration.

The left panel of Figure 3 illustrates a favorable source trajectory found in this way. In this and the following examples, the distance between source and isocenter is 810 mm, and the radius of B_0 is about 125 mm. The right panel of Figure 3 shows 28 umbrella-shaped surfaces within B_0 , as described in Section 3. As can be seen, this trajectory is complete. Figure 4 illustrates four additional complete trajectories. The angular functions for all five example trajectories are given in Table 1. The definitions involve some magic constants which depend on the geometrical parameters of the underlying C-arm system. As indicated in the table, these example trajectories have various merits and may impose additional technical requirements on the C-arm system.

As with a circular arc, the true trajectory will deviate a little from the prescribed trajectory, but these deviations can be measured and taken into account during the reconstruction. With high-end C-arm systems the deviations are also reproducible.

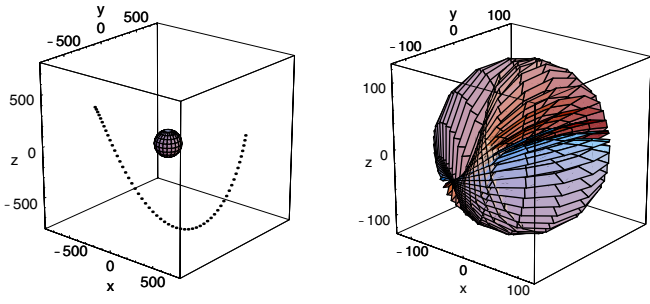


Figure 3. A complete source trajectory. The small ball in the left panel represents B_0 . The right panel illustrates the filling of B_0 with umbrella-shaped surfaces, as described in Section 3.

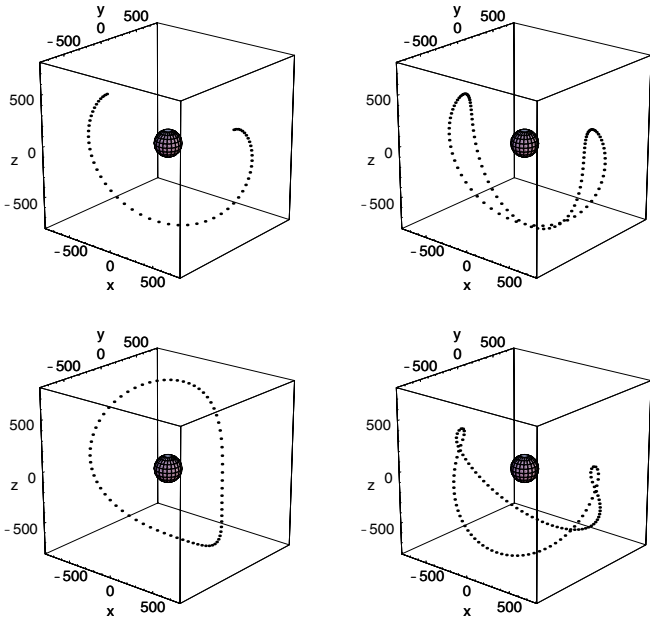


Figure 4. Four additional complete source trajectories.

Illustration	Definition ($0 \leq \lambda \leq 1$)	Comments
Figure 3	$\theta_1(\lambda) = -\frac{\pi}{180} 36$ $\theta_2(\lambda) = \frac{\pi}{180} (22.5 - 225\lambda)$ $\theta_3(\lambda) = \frac{\pi}{180} (45 - 90\lambda)$	L-arm at -36° θ_1, θ_2 linear
Figure 4 top left	$\theta_1(\lambda) = 0$ $\theta_2(\lambda) = \frac{\pi}{180} (22.5 - 225 \sin^2(\pi\lambda/2))$ $\theta_3(\lambda) = \frac{\pi}{180} 18 \sin(2\pi\lambda)$	L-arm at 0°
Figure 4 top right	$\theta_1(\lambda) = 0$ $\theta_2(\lambda) = \frac{\pi}{180} (22.5 - 225 \sin^2(\pi\lambda))$ $\theta_3(\lambda) = \frac{\pi}{180} 12 \sin(4\pi\lambda)$	L-arm at 0° trajectory closed
Figure 4 bottom left	$\theta_1(\lambda) = 0$ $\theta_2(\lambda) = \frac{\pi}{180} (-90 - 360\lambda)$ $\theta_3(\lambda) = \frac{\pi}{180} 15 \cos(4\pi\lambda)$	L-arm at 0° trajectory closed requires 360° rotation for j_2
Figure 4 bottom right	$\theta_1(\lambda) = -\frac{\pi}{180} 90$ $\theta_2(\lambda) = \frac{\pi}{180} a_2(\lambda)$ $\theta_3(\lambda) = \frac{\pi}{180} a_3(\lambda)$	L-arm at -90° trajectory closed a_2, a_3 shown in Figure 5 requires 210° rotation for j_3

Table 1. The definitions of the five example trajectories.

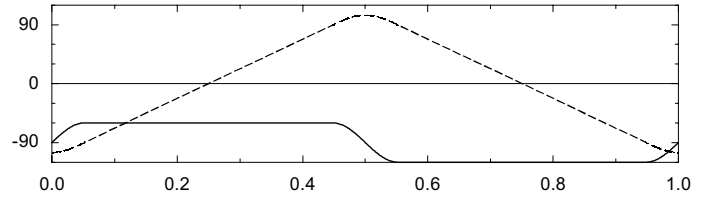


Figure 5. The functions a_2 (solid) and a_3 (dashed) referenced in the last row of Table 1.

References

- [1] M. Grass, R. Koppe, E. Klotz, R. Proksa, M. H. Kuhn, H. Aerts, and J. Op de Beek, "Three-dimensional reconstruction of high contrast objects using C-arm image intensifier projection data," *Computerized Medical Imaging and Graphics*, vol. 23, pp. 311–321, 1999.
- [2] K. Wiesent, K. Barth, N. Navab, T. Brunner, O. Schuetz, and W. Seissler, "Enhanced 3D-reconstruction algorithms for C-arm systems suitable for interventional procedures," *IEEE Transactions on Medical Imaging*, vol. 19, no. 5, pp. 391–403, May 2000.
- [3] L. A. Feldkamp, L. C. Davis, and W. J. Kress, "Practical cone-beam algorithm," *J. Opt. Soc. Amer. A*, vol. 1, no. 6, pp. 612–619, June 1984.
- [4] C. Hamaker, K. T. Smith, D. C. Solmon, and S. L. Wagner, "The divergent beam X-ray transform," *Rocky Mountain Journal of Mathematics*, vol. 10, no. 1, pp. 253–283, 1980.
- [5] R. Koppe, E. Klotz, J. Op de Beek, and H. Aerts, "3D vessel reconstruction based on rotational angiography," in *CAR '95: Computer Assisted Radiology and Surgery*, H. U. Lemke, K. Inamura, C. C. Jaffe, and M. W. Vannier, Eds. 1995, pp. 101–107, Springer.
- [6] R. Fahrig and D. W. Holdsworth, "Three-dimensional computed tomographic reconstruction using a C-arm mounted XRII: Image-based correctin of gantry motion nonidealities," *Medical Physics*, vol. 27, no. 1, pp. 30–38, January 2000.
- [7] R. Clack and M. Defrise, "Cone-beam reconstruction by the use of Radon transform intermediate functions," *J. Opt. Soc. Amer. A*, vol. 11, no. 2, pp. 580–585, February 1994.
- [8] M. Defrise and R. Clack, "A cone-beam reconstruction algorithm using shift-variant filtering and cone-beam back-projection," *IEEE Trans. Med. Imag.*, vol. 13, no. 1, pp. 186–195, March 1994.
- [9] R. M. Lewitt, "Processing of incomplete measurement data in computed tomography," *Medical Physics.*, vol. 6, no. 5, pp. 412–417, 1979.
- [10] M. W. Spong and M. Vidyasagar, *Robot Dynamics and Control*, John Wiley & Sons, 1989.